GA–A25930

# PROGRESS IN CHARACTERIZATION OF THE H-MODE PEDESTAL

by
A.W. LEONARD

SEPTEMBER 2007

GENERAL ATOMICS

# DISCLAIMER

GA–A25930

# PROGRESS IN CHARACTERIZATION OF THE H-MODE PEDESTAL

by
A.W. LEONARD

This is a preprint of a review paper to be presented at the 11th IAEA Technical Meeting on H-Mode Physics and Transport Barriers, in Tsukuba, Japan on September 26-28, 2007 and to be published in the *Proceedings.*

Work supported by
the U.S. Department of Energy
under DE-FC02-04ER54698

GENERAL ATOMICS PROJECT 30200
SEPTEMBER 2007

# ABSTRACT

The H-mode pedestal remains a critical subject for magnetic fusion energy research. Recent experimental efforts to characterize the edge pedestal, for tests of pedestal models now under development, are summarized in this report. The pedestal transport is characterized by the profiles and energy and particle fluxes through both the electron and ion channels. The flux measurements are made difficult by the short scale lengths of the pedestal and the difficulty of measuring the neutral ionization source within the pedestal. Recent results on pedestal scaling with a number of parameters are also summarized. Measurements of the pedestal scaling with the ion gyroradius, global beta, input power, shape, critical gradients, neutral density, aspect ratio, rotation, toroidal ripple and the toroidal field direction are presented. These measurements provide a strong test for emerging pedestal models as well as improve confidence of extrapolating existing experiments towards future devices. Recent work on the scaling of the H-mode power threshold is also presented.

# INTRODUCTION

The H-mode pedestal, a narrow region of reduced transport near the plasma edge, remains a critical issue for magnetic fusion energy research. For the core plasma the edge pedestal serves as a boundary condition for the central density and temperature profiles. With improved models of core plasma transport, the H-mode edge pedestal conditions now represent the largest uncertainty in predicting the performance of future burning plasma experiments [1,2]. The pedestal region also represents a boundary condition for the scrape off layer (SOL) plasma. Models of the SOL, important for predicting the heat flux onto the plasma facing component, require the poloidal distribution of heat and particle flux across the separatrix. A complete and validated pedestal model will be required to predict the details of these fluxes. Finally, the plasma conditions required for accessing the H-mode regime are an important aspect for the design of future devices. Access to H-mode is critical for a burning plasma tokamak such as ITER and thus any reduction in uncertainty could result in improved design flexibility and increased confidence in achieving performance goals. All of these issues indicate the high priority of developing a pedestal model with predictive capability.

Development of the peeling-ballooning model [3-5] for the MHD stability limit of the pedestal has provided a powerful constraint on predictions for the achievable pedestal height in a given configuration. The peeling-ballooning model describes a limit for the edge pressure gradient and current that build in the pedestal region during H-mode. The edge gradients build in the pedestal until the MHD limit is reached and an edge localized mode (ELM) typically results. After an ELM the gradients build again until the next ELM. While these models make certain assumptions, such as exclusion of the plasma very near the separatrix, the peeling-ballooning MHD limit has been tested in a number of configurations and conditions with generally good agreement within experimental uncertainty. An example of this agreement taken from reference [4] is shown in figure 1. In this case pedestal electron density and temperature profiles were selected just before an ELM in a set of discharges from DIII-D with a wide density range, but at constant plasma current, field, shape and pedestal width. The stability limit of these discharges was estimated with the ELITE code [5] and a series of magnetic equilibria with increasing pedestal temperature for the experimental configuration, density and pedestal width. In each case examined the pedestal temperature at which the equilibrium becomes unstable was in agreement with the observed pedestal temperature. The pedestal width is an important aspect of the analysis as numerical studies have found the critical pressure gradient to decrease with pedestal width as $p' \propto \Delta^{-1/4}$, where $\Delta$ is the width of a hyperbolic tangent function used to parameterize the pedestal pressure profile [5]. With the success of the peeling-ballooning model the calculation of pedestal height in future devices then relies upon a predictive capability for the width of the pedestal steep pressure gradient region.

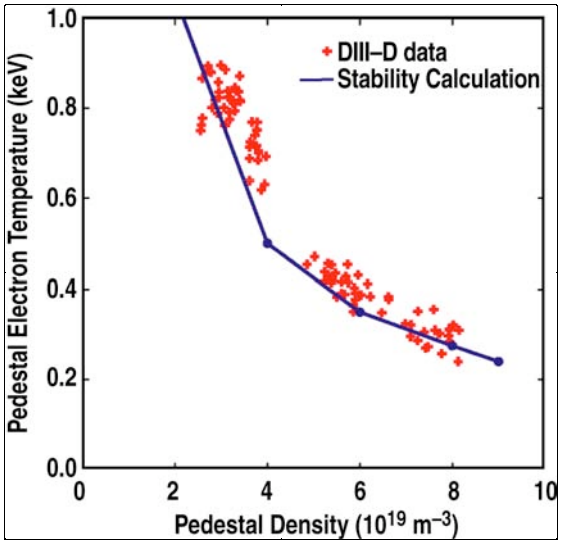


Fig. 1. Comparison of pedestal stability limit calculated with ELITE to DIII-D data as a function of pedestal density. (Reprinted with permission from Snyder P B 2004 *Plasma Phys Control Fusion* **46** A131. Copyright 2004, Institute of Physics.)

In order to improve predictive capability for the pedestal width, and thus its height, a multi-device pedestal database was established by the ITPA Pedestal Topical Group [6]. This database contains pedestal measurements from many of the tokamaks in the world fusion research community. There are several shortcomings when examining the scaling of this database, primarily that the tokamaks all have different measurement characteristics and capabilities for the pedestal. Several devices could not measure both the pedestal electron density and temperature profiles simultaneously with the pedestal ion temperature. In these cases analysis of the database required setting equal the ion and electron pedestal profiles. Also the pedestal is narrow and its width cannot be resolved in many cases so only the pedestal height can be examined. Given these shortcomings, several studies examined the ITPA database for scaling of the pedestal top pressure [7-9]. While these studies included different analysis techniques, such as utilizing stability constraints, all found significant uncertainty when projecting their respective scaling results to ITER.

The difficulty in producing a scaling relationship from a pedestal database is illustrated in a study of the ITPA database using theory-based models to examine the pedestal width [10]. Because only the pedestal pressure top was generally available the width was obtained from an analytic MHD stability constraint. The derived widths were then fit to a number of proposed theories for the pedestal width. The theory based models examined included the width being set by: i) magnetic and shear flow stabilization, $\Delta \propto \rho S$, ii) flow shear stabilization, $\Delta \propto \sqrt{\rho R q}$, iii) diamagnetic stabilization, $\Delta \propto \rho^{2/3} R^{1/3}$, iv) neutral penetration, $\Delta \propto 1/n_{\mathrm{ped}}^{3/2}$, v) ion orbit loss, $\Delta \propto \sqrt{\varepsilon}\rho_\theta$, and vi) normalized poloidal pressure, $\Delta \propto \sqrt{\beta_\theta} R$, where $\Delta$ is the pedestal width, $\rho$ is the ion gyroradius, $S$ is the magnetic shear at the pedestal top, $R$ is the major radius, $q$ the safety factor, $n_{\mathrm{ped}}$ the pedestal density, $\varepsilon$ the aspect ratio, $\rho_\theta$ the

ion poloidal gyro-radius, and $\beta_p$ the pedestal pressure normalized by the poloidal field. As can be seen from a summary of the different model fits to the data in Table 1, most of the model fits to the data are of equal quality. Of particular concern in this database exercise is that the models have a very different dependence on ion gyroradius, ranging from linear dependence to independent of gyroradius, with a similar quality fit to the data. The ion gyroradius is the one parameter that current experiments cannot match the expected values in a burning plasma class tokamak. The range of gyroradius dependence implies an uncertainty of a factor of 2, or greater, when projecting the pedestal height to a tokamak such as ITER.

**Table 1**
**Root Mean Square Error (RMSE) in Fit of the ITPA Database to Different Models of the Pedestal Width**

| Model | Width | RMSE (%) |
|---|---|---|
| Magnetic and flow shear | $\Delta \propto \rho S$ | 32 |
| Shear flow | $\Delta \propto \sqrt{\rho R q}$ | 30.8 |
| Diamagnetic stabilization | $\Delta \propto \rho^{2/3} R^{1/3}$ | 33.7 |
| Neutral penetration | $\Delta \propto 1/n_{ped}^{3/2}$ | 53.4 |
| Ion orbit loss | $\Delta \propto \sqrt{\varepsilon \rho_\theta}$ | 34.4 |
| Poloidal pressure | $\Delta \propto \sqrt{\beta_\theta} R$ | 32.9 |

The difficulty in distinguishing simple models by use of the database arises not only from the measurements as described earlier, but also from the assumptions made by these models. The pedestal location, just inside the separatrix, is a region of varying shape and magnetic shear that may depart significantly from analytic approximations. Also the analytic approximations for neoclassical ion transport may not be valid due to the radial electric field and separatrix geometry. In addition, most models of pedestal transport assume equilibrium, while as described above the pedestal is continually evolving from one ELM to the next violating this assumption of steady state. Finally the pedestal particle source is not poloidally uniform due to edge and divertor recycling. This non-uniform particle source could result in 2D transport issues for which models will have to account.

All of the complicating factors outlined above motivate a more careful and dedicated approach to developing a validated pedestal model that can be used with confidence to predict pedestal performance in future tokamaks. To directly test newer pedestal transport models that are under development documentation is required of the profiles of all relevant parameters, including both the electrons and ions and their fluctuations as well as the energy and particle flux through both channels. A second valuable approach is to measure changes in pedestal parameters across single parameter scans. Dedicated experimental scans can bring out trends that may be masked by incomplete data sets and correlated parameters in typical database studies. The trends obtained in dedicated experimental scans can be used to guide

and validate model development as well as for developing empirical scaling relations for pedestal prediction in future tokamaks.

This report summarizes the current status, and recent progress in experimental characterization of the H-mode pedestal and criteria for H-mode access. In particular, areas that require further work to facilitate progress in edge pedestal model development will be highlighted. In section 2, progress characterizing transport through the pedestal will be described. These measurements will be important to test more complete models of the pedestal that are now under development. Section 3 will survey recent experiments that seek to illuminate the underlying physics controlling the pedestal height through single parameter scans in individual devices and cross device comparisons. The consistent trends observed in these experiments can serve to guide and validate pedestal model development. In section 5 some recent progress in H-mode power threshold scaling will be summarized. Finally section 6 will summarize progress in pedestal research and highlight high priority topics required for further progress.

## 2. CHARACTERIZATION OF PEDESTAL TRANSPORT

New code models of pedestal transport now under development will capture many aspects of physics relevant to transport in the edge pedestal region. The code TGLF [11,12] uses quasi-linear approximations to full gyrokinetic simulation of driftwave turbulence that can be active in the pedestal region. In addition the code uses realistic separatrix geometry and includes other pedestal effects such as collisions and a description of neoclassical ion transport. The TGLF code is now at the stage of computing growth rates of instabilities for measured pedestal profiles. The code GEM [13,14] is modeling full turbulence in the edge and finding that electromagnetic turbulence must be included along with electrostatic in order to accurately model edge transport. An ambitious approach is being taken by the codes TEMPEST [15] and XGC-1 [16]. These codes are implementing a full gyrokinetic simulation of the pedestal and SOL region to encompass all the relevant physics. The TEMPEST code is taking a continuum approach while the XGC-1 is using a particle-in-cell (PIC) method to describe transport. Both codes will employ self-consistent neoclassical transport that will take into account the self-generated radial electric field in the edge pedestal. The codes will also model realistic recycling neutral particles to accurately model the particle source. Already these codes are showing the potential of neoclassical transport to drive a pedestal radial electric field and determine much of the pedestal characteristics [15,17]. An accurate model for turbulent electron transport must still be added before the simulations can be directly compared to experiment.

All of the pedestal modeling codes described above need accurate pedestal characterization to guide their development and validate their results. The most basic characterization of a pedestal transport model is the ion and electron profiles of density and temperature and the radial energy and particle flux profile through these two species. Several SOL and divertor fluid modeling codes, such as SOLPS [18], UEDGE [19] and EDGE2D [20], encompass the pedestal region and can be used to characterize transport in the pedestal. However, these codes are typically utilized in a predictive mode with preset transport characteristics. Interpretive transport analysis, such as the example shown in figure 2 [21], is generally more useful for determining energy and particle source terms, and then calculating the corresponding fluxes through the continuity equation. The interior energy source, which flows radially through the pedestal, is typically straightforward to determine from ohmic and auxiliary heating analysis. However within the pedestal significant radial energy flux can be transferred from the ions to the electrons due to a stronger gradient in the pedestal electron temperature. This is illustrated in figure 2(a) and can result in significant changes to the radial energy flux profiles. An accurate determination of the separate energy fluxes through the electrons ($Q_e$) and ions ($Q_i$) then requires that both of their respective profiles be resolved through the entire pedestal region.

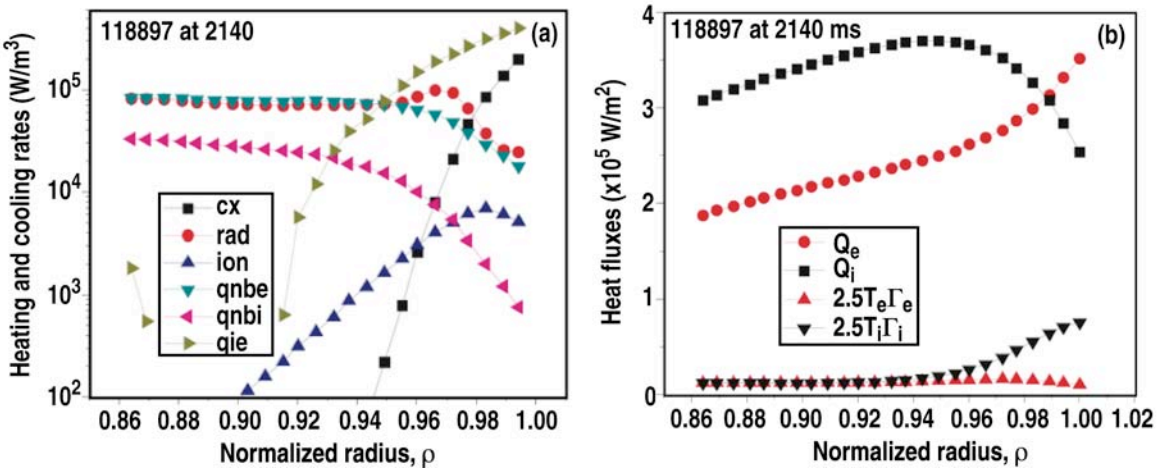


Fig. 2. (a) Heating and cooling rates during ELM-free H-mode in the pedestal region of DIII-D (cx = charge-exchange+elastic scattering cooling, rad = radiation cooling, qnbe = neutral beam heating of electrons, qnbi = neutral beam heating of ions, qie = collisional energy exchange from ions to electrons). (b) Total electron (Qe) heat flux, ion heat flux (Qi) and convective heat fluxes for both ions and electrons during ELM-free H-mode in the pedestal region. (Reprinted with permission from Stacey W M 2007 *Phys Plasmas* **14** 012501. Copyright 2007, American Institute of Physics.)

Time dependence is another critical issue for characterising pedestal transport as the profiles evolve from one ELM to the next. This is particularly true for pedestal diagnostics that can vary in time response from the almost instantaneous Thomson scattering measurement, to much slower ion temperature measurements from CER. For some applications, such as stability analysis, profiles just before an ELM are required, while for others, such as implications for core confinement, averaging over the ELM cycle is more appropriate. For transport analysis evolution of the profiles between ELMs is required. While the example in figure 2 is averaged over the ELM cycle, further analysis of the same discharge [22] has indicated that the change in stored energy, dW/dt, and particles, dn/dt, can significantly change the energy and particle flux in the pedestal from that inferred from time averaged profiles.

Determination of the pedestal particle flux is more problematic. This is because a large fraction of pedestal particle flux arises from neutral ionization within the pedestal region itself due to the SOL and divertor recycling source. This effect can be seen in figure 2(b) where the convective ion energy flux ($2.5T_i\Gamma_i$) greatly increases within the pedestal region. In addition, as shown in figure 2(a), the edge recycling neutrals can cause significant charge-exchange loss to the energy transported radially through the ion channel. While the neutral ionization and density in figure 2 is determined from a more sophisticated 2-point SOL and divertor model, than is used in typical transport analysis, a significant uncertainty still exists. A more accurate determination of the 2D profile of neutral density within the pedestal is required to address these uncertainties.

The uncertainty in determining the profile of neutral ionization and density within the pedestal arises from several factors. Because the direct measurement of neutral density within a plasma is difficult, neutral ionization is usually determined by spectroscopic measurements with the neutral density inferred from these measurements using the measured pedestal densities and temperatures. These spectroscopic measurements are difficult firstly because the line of sight measurements require inversion of a hollow profile where the pedestal emission is much less than in the surrounding SOL and divertor. Secondly, interpretation of the most common measurements of ionization, $D_\alpha$ emission, is subject to large uncertainties due to the strong dependence of the emission rate on the background plasma density and temperature. While ionization measurements based on $Ly_\alpha$ emission is less dependent on the background plasma [23], implementing a 2D $Ly_\alpha$ diagnostic is technically challenging and expensive, and thus may not be widely deployable. A 2D measurement of the ionization profile is required because of the very strong local neutral source in the divertor compared to the main chamber. This can lead to a very different width of the ionization profile depending on the assumed location of the dominant recycling when the flux expansion from the midplane to the divertor can be a factor of 5.

One approach to determining the neutral density and ionization profile is through interpretive modeling. With this concept one first obtains a neutral particle flux from all of the plasma facing surfaces equal to the ion flux profile onto these surfaces. The ion flux profile to all surfaces can be determined by measuring the flux profile in the divertor and selected main chamber locations with fixed Langmuir probes. The complete ion flux profile can then be interpolated using the decay length of the plasma density and temperature in the SOL and assuming sonic plasma flow to surfaces [24]. Initial analysis of this kind has indicated that the total main chamber ion flux is the same order as the divertor ion flux [24-26]. The inferred neutral flux from plasma facing surfaces can then be converted to an ionization profile through a Monte Carlo simulation, which launches the same profile of neutral flux into a reconstructed plasma background that matches the experimental conditions. The reconstructed plasma background can be obtained by a fluid model of the pedestal and boundary plasma, such as UEDGE, SOLPS, EDGE2D or OSM [27], constrained by as many experimental measurements as possible. The resulting 2D profile of ionization can then be checked for consistency with profiles of $D_\alpha$ recycling emission. The uncertainties with this approach arise from the accuracy of the reconstructed plasma background and the assumption of saturated walls where the ion flux matches the neutral flux.

An example of this type of interpretive modeling is shown in figure 3 [28]. The 2D $D_\alpha$ taken at a time in between ELMs, figure 3(a), clearly shows how the emission is peaked outside the separatrix, particularly in the divertor. The poloidal profile of neutrals crossing the separatrix, figure 3(b), obtained from a Monte Carlo simulation, indicates the divertor region represents the largest source of ionization fueling the pedestal. There is still significant

development work needed however. In the example given, the Monte-Carlo wall neutral flux has not yet been made consistent with the wall ion flux profile. In addition a sensitivity study is needed to determine the dependence of the inferred ionization profile on uncertainties in the reconstructed plasma background. Finally time dependence of the ionization profile should be addressed. Particularly it has been shown that during an ELM the wall ion flux can be very large and with a very different profile than the quiescent period between ELMs [26]. The ion radial flux during ELMs typically represents 20%-40% of the total radial ion flux across the separatrix [26,29] and will need to be taken into account.

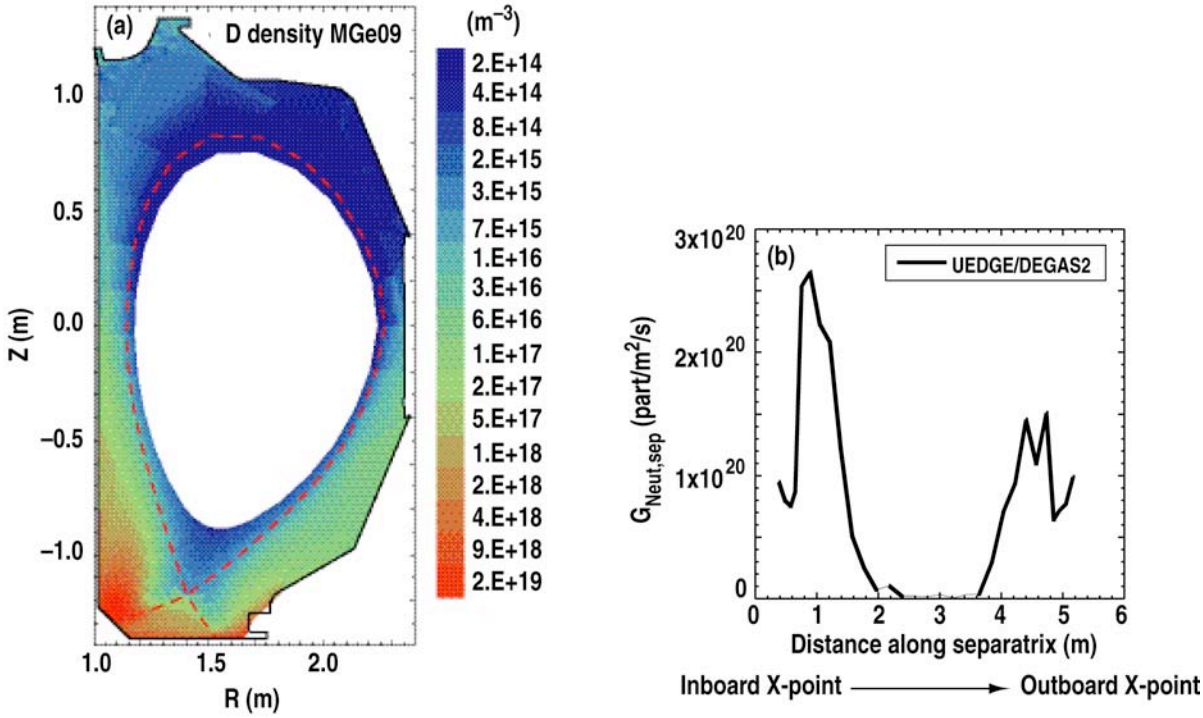


Fig. 3. (a) The neutral deuterium density as simulated by UEDGE constrained by experimental measurements. (b) The Monte-Carlo (DEGAS) calculated neutral flux across the separatrix in H-mode as a function of poloidal angle. (Groth M *et al* 2005 *J Nucl Mater* **337-339** 425)

Other profiles are also important for testing pedestal transport models. The fluctuation characteristics within the pedestal are important for validating the physics within models of the pedestal. The pedestal arises in a region where the naturally occurring fluctuation-driven transport is reduced. Earlier data has shown that the region of edge fluctuation suppression in H-mode corresponds roughly to the steep gradient region in the pedestal [30-32]. Further work is required to determine if the fluctuation suppression corresponds to the region of steep temperature gradient. Also measurements of the residual fluctuations in the pedestal will be valuable for testing models of pedestal transport that sets the electron and ion temperature gradients.

The magnetic shear is another important characteristic of the pedestal that is needed to test models. The magnetic shear in the pedestal is important firstly because it is an important parameter determining the stability limit of the peeling-ballooning model. A lower magnetic shear stabilizes the pressure driven modes that lead to an ELM and limit the growth of the pedestal pressure. The shear is also an important parameter for pedestal transport. Theoretical considerations suggest it may play a role in setting the pedestal width [33]. Variation in the pedestal magnetic shear arises because of the edge bootstrap current that is driven by the steep gradients in the pedestal [34]. Initial measurements of the pedestal bootstrap current find it consistent with a neoclassical collisional bootstrap current model [35,36]. Most of these measurements are taken during long ELM-free periods for better averaging. Additional measurements are needed to characterize the pedestal bootstrap current and resulting magnetic shear in the presence of ELMs that may dissipate some of the edge current.

# 3. EXPERIMENTAL SCALING OF THE PEDESTAL HEIGHT AND WIDTH

Another important approach to experimental characterization of the pedestal is empirical scaling of controlling parameters. This approach can illuminate the important physical processes controlling the pedestal and reveal effects that must be included in any pedestal model. Single parameter scans can provide an important test for pedestal models to exhibit the same trends. Also empirical scaling can be used in its own right to predict pedestal characteristics in future tokamaks and lend confidence to model predictions for those devices.

In contrast to multi-machine pedestal database studies, with their significant uncertainties in scaling, recent experiments dedicated to varying single parameters and cross-machine comparisons are now yielding consistent trends in pedestal characteristics. With the advance of pedestal peeling-ballooning stability models these trends can now be analyzed to separate the contribution of MHD stability from pedestal width changes to the pedestal height.

In the following section recent pedestal scaling experiments will be summarized. The parameters varied in these studies include the ion gyroradius, injected power, global beta, plasma shape, neutral density, critical gradient scale lengths and toroidal ripple. The scaling results will be examined in terms of the important physical processes that should be included in any accurate pedestal model.

## 3.1. ION GYRORADIUS

The ion gyroradius, $\rho^*$, is an important scaling parameter because it is the one dimensionless parameter of a burning plasma scale tokamak that cannot be reproduced in current experiments. Projections to future larger tokamaks such as ITER rely upon extrapolation of experimental scaling of $\rho^*$ from current tokamaks and theoretical models based upon validated physics. As mentioned in the introduction a number of theories of pedestal width, and thus height, predict different dependencies upon $\rho^*$. For theories based upon pressure driven flow shear suppression of edge turbulence the $\rho^*$ dependence could range from $\rho^{1/2}$ to $\rho^1$, depending upon details of the dominant turbulence and suppression mechanism [23,37,38]. For theories based upon ion orbit loss setting up a radial electric field shear to suppress turbulence the width should scale as the poloidal ion gyroradius, $\rho_\theta$ [39], or possibly the toroidal ion gyroradius in the case of orbit squeezing due to the self-consistent radial electric field [40]. Other theoretical considerations [41] would even suggest no dependence of the pedestal width on ion gyroradius. These different $\rho^*$ dependencies project to a factor of two or more uncertainty in the pedestal height of ITER.

An early experiment in DIII-D found no change to the pedestal width, or height, when $\rho^*$ was varied by a density scan [42]. However other parameters such as pedestal collisionality, $\nu^*$, were not kept constant. Because the pedestal height may vary with other parameters, such

as shape and plasma beta, that affect the pedestal stability limit, it is important to carry out experimental scans of $\rho^*$ with all other dimensionless parameters held fixed. Another examination of $\rho^*$ scaling was carried out in a cross-machine comparison between JET and DIII-D [43]. The pedestal widths as a function of $\rho^*$ just before an ELM is shown in figure 4. In this comparison when $\beta$, $\nu^*$ and $\rho^*$ were matched at the top of the pedestal the normalized width of the transport barrier, as parameterized by a hyperbolic tangent fit to the pedestal electron temperature, $\Delta_T$, was similar in both devices. Other comparison experiments have also found the transport barrier width to remain constant when keeping the dimensionless parameters fixed [44,45]. For the comparison in figure 4 the pedestal density was higher in DIII-D in order to match the dimensionless parameters. This resulted in a narrower pedestal density width in DIII-D, consistent with a shorter neutral penetration length. The scaling with density will be described in section 3.4. In DIII-D $\rho^*$ was scanned from the matched condition to one with $\rho^*$ larger by a factor of 1.6, while only a 15% variation in $\rho^*$ was achieved in JET. Over this range of $\rho^*$ no consistent change in the transport barrier width was observed, as shown in figure 4.

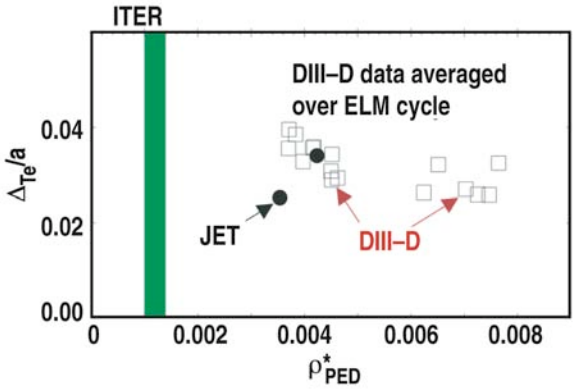


Fig. 4. The electron temperature pedestal width normalized by the minor radius in JET and DIII-D as a function of the toroidal ion gyroradius also normalized by the minor radius. Other dimensionless parameters are kept constant including shape, collisionality and beta.

The implications of the observed lack of $\rho^*$ dependence for the pedestal width are significant. This scaling would imply a wider, and higher, pedestal in ITER than would otherwise be expected, resulting in higher confinement and significantly better performance. In addition many theories of H-mode transport suppression would have to be revised to accommodate this scaling. Obviously future experiments across devices are of high priority to address this issue.

### 3.2. INPUT POWER AND GLOBAL BETA

In a transport model where gradients are driven by fluxes it is typical to scale the pressure with power flowing through the region. With this motivation an examination of the ITPA pedestal database [9] found $W_{ped}$ the pedestal energy as defined by the pedestal top pressure times the plasma volume, to increase with power as in the following expression:

$$W_{ped} = 0.00807\, I_p^{1.41}\, R^{1.37} P^{0.50}\, n_e^{-0.15}\, B_t^{0.32}\, m^{0.2}\, F_q^{1.61}\, \kappa_a^{1.21}\ , \qquad (1)$$

where $I_p$ is the plasma current $R$ is the major radius, $P$ the thermal loss power, $n_e$ the density, $B_t$ the toroidal field, $m$ the atomic mass, $\kappa_a$ the elongation and $F_q = q_{95}/q_{cyl}$ where $q_{cyl} = 5\,\kappa a^2 B_t/RI_p$. Another ITPA study [46] examined carefully selected profiles from ASDEX-Upgrade, JET, JT-60U and DIII-D in ELMing H-mode and found $W_{ped}$ to increase with input power consistent with the earlier study. Further examination of the dataset revealed the normalized poloidal beta, $\beta_{pol}$, at the top of the pedestal was also strongly correlated with the total, or global, $\beta_{pol}$, as shown in figure 5. For this dataset the pedestal $\beta_{pol}$ was averaged over the ELM cycle to examine the implications for core plasma confinement.

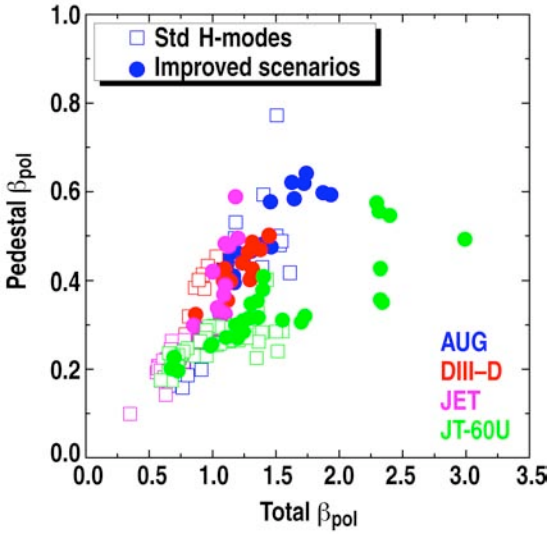


Fig. 5. Pedestal $\beta_{pol}$ versus global $\beta_{pol}$ for H-mode discharges in AUG, DIII-D, JET and JT-60U. Standard H-mode discharges are shown with open symbols and discharges in advanced regimes are indicated by closed symbols. (Reprinted with permission from Maggi C F 2007 *Nucl Fusion* **47** 535. Copyright 2007, Institute of Physics.)

In the peeling-ballooning model the pedestal pressure gradient, and thus the top of the pedestal, is limited by the MHD stability limit. This limit is dependent on a number of factors including, pedestal width, shape, plasma current, toroidal field density and temperature. The influence of these factors can be seen in the dependencies of the scaling in equation 1. In addition at least part of the power dependence can be attributed to an increase in the pedestal stability limit. Experiment and stability modeling has documented that higher poloidal beta, and the resulting Shafranov shift, due to higher heating power can significantly raise the pedestal gradient stability limit [47]. This effect is stronger in more highly shaped plasmas and may add to the shaping dependence.

In addition to an increase in the pedestal pressure gradient, the pedestal width has also been found to increase at higher input power and/or global beta [46,48,49]. This results in an even greater increase in the pedestal pressure with β than would be expected from the stability increase alone. The width increase is most apparent in the pedestal ion temperature, but the electron temperature width is increased as well. The underlying physical cause for this increase in width is not yet established, but several candidate mechanisms are possible. First, the increase in stability limit at higher β could allow for a higher ion temperature, or greater $\rho^*$. This could lead to a greater width of the pedestal transport suppression region as described by several theories. Another possibility is that simply the greater energy flux

through the pedestal at higher beta could increase the width of transport suppression as described in reference [38]. Or alternatively the increase in pedestal pressure gradient at high β could modify the magnetic shear profile in the edge increasing the spatial region over which conditions for H-mode transport suppression are met. It is important to resolve which of these mechanisms are responsible for the increase in width with β and/or power as they have different implications for scaling to larger tokamaks, particularly for advanced scenarios that aim to operate at high β.

### 3.3. PLASMA SHAPE

It has long been recognized that plasma shape can significantly affect the height of the H-mode pedestal in a tokamak. Increasing triangularity has yielded higher global confinement in ELMing H-mode, particularly at higher density, in a number of tokamaks [50-52]. This has generally been understood as higher triangularity allowing for a higher pedestal pressure through a higher MHD stability limit in the peeling-ballooning model [4,5]. Higher moments of the shape, such as squareness and location of a secondary separatrix, can also significantly affect pedestal stability [49]. While a few stability studies have parameterized the stability limit with respect to basic parameters of shape much more work is required to quantify the stability effects of other aspects of shape such as the separate influence of upper and lower triangularity, higher moments of the shape, and location of the secondary X-point.

An examination of two plasmas with different squareness in DIII-D, but otherwise similar conditions revealed that the influence of shaping on pedestal structure can extend beyond changes to the MHD stability limit [49]. The two shapes shown in figure 6(a), with otherwise constant conditions, produced the pedestal profiles just before an ELM as shown in figure 6(b). This example shows how a modest change in shape can produce a significant increase in pedestal pressure. Stability analysis of these shapes using pedestal profiles of the same width, as parameterized by a hyperbolic tangent function, revealed that only half of the measured increase in pedestal top pressure could be attributed to the improved stability limit of the less square shape. The other half of the increase of the pedestal is presumably from an increase in the pedestal width. Because of the limited spatial resolution of the diagnostics in the narrow pedestal the uncertainty in the measurement of the pedestal width is typically much larger than that of the pedestal height. This type of analysis uses the validated stability model to constrain the pedestal measurements and thus obtain a better assessment of variation in the pedestal width for what would otherwise be a difficult measurement.

The issue of pedestal width variation with shape is very similar to that for global β as described in section 3.2. The increase in width with stronger shaping could be due to an increasing $\rho^*$ as the improved stability limit allows higher pressure. Or, the effect of the shape could broaden the region where the conditions are met for H-mode suppression of turbulent transport. Understanding these mechanisms will be required to improve confidence in models and scaling results to future larger tokamaks.

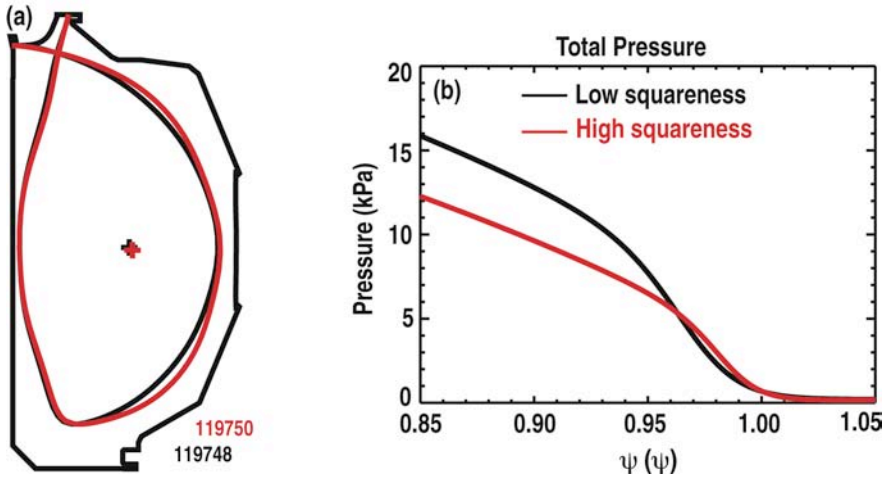


Fig. 6. Modest change in the discharge shape squareness (a) produces a significant change in the pedestal pressure profile. (Reprinted with permission from Leonard A W 2007 *Nucl Fusion* **47** 552. Copyright 2007, Institute of Physics.)

### 3.4. NEUTRAL DENSITY IN THE PEDESTAL

The particle ionization source within the pedestal itself due to recycling neutrals can also affect the structure of the pedestal. It is generally expected that the pedestal density profile and its gradient result from the convolution of this particle source with the underlying transport. In addition theoretical considerations suggest that the particle flux from this source could be one of the factors driving the H-mode transport barrier formation [38]. An additional motivation for studying the pedestal density profile separately is its role in obtaining burning plasma conditions in the core plasma. Because neutral penetration of recycling neutrals will be much less in a large burning plasma tokamak than in current devices central fueling through pellet injection is envisioned. The role of the edge pedestal in setting the core density profile will be an important factor in obtaining burning plasma conditions.

As described earlier in section 2, an accurate measurement of the 2D ionization profile in the pedestal is not generally available in current experiments. To address the issues of neutrals a number of scaling experiments and cross-machine comparisons have been carried out and compared to reduced models of edge recycling and particle transport. An earlier scaling study in DIII-D found the pedestal density width to scale inversely with the pedestal density height [42,53]. This is in rough agreement with a simple model of neutral penetration and particle continuity in the plasma edge where the pedestal ionization source is balanced by outward particle flux. This study also found that the pedestal temperature width was similar to the density width in most instances. A follow-on experiment constructed a dimensionless parameter comparison between DIII-D and Alcator C-Mod (C-Mod) [44]. Because of the higher field and density in C-Mod a simple neutral penetration model would expect a smaller normalized pedestal width in C-Mod. However, as shown in figure 7 where the DIII-D

density and temperature profiles were normalized to match the C-Mod dimensionless parameters, the normalized density width was very similar in both devices. Other studies have produced mixed results, with ASDEX-Upgrade [54] finding a constant pedestal density width over a range of densities while JET [55] and MAST have found the density width to scale as expected from a more detailed neutrals model [56].

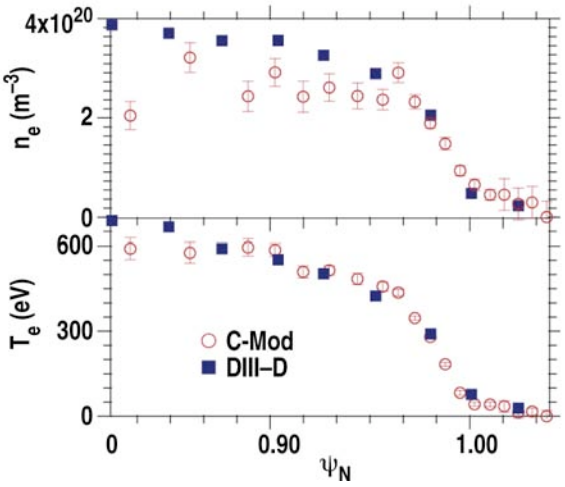


Fig. 7. Dimensionless comparison of pedestal profiles in C-Mod and DIII-D. The DIII-D profiles are normalized to match the dimensionless parameters of ion gyroradius, collisionality and β. (Reprinted with permission from Mossessian D A 2003 *Phys Plasmas* **10** 689. Copyright 2003, American Institute of Physics.)

Several competing effects could explain some of the ambiguous results of pedestal density width scaling. For pedestal fueling dominated by the X-point region, as suggested in some DIII-D studies [28], the flux expansion is larger resulting in a shorter normalized neutral penetration length than if the recycling is poloidally symmetric. It has been postulated that the higher density and metal surfaces of C-Mod could lead to more poloidally symmetric pedestal fueling compared to the lower density and carbons surfaces of DIII-D and lead to similar normalized density profiles. Other effects that must be taken into account are the kinetic details of neutral transport and ionization. A 1-D kinetic neutrals model [57] found that while the density width should be inversely proportional to the pedestal density at DIII-D conditions, over the range of the higher C-Mod pedestal density the pedestal density width could be independent of density [58]. Finally simple 1-D pedestal density scaling studies have indicated that either the neutral penetration length or the transport barrier width could set the pedestal density width depending on the regime and relative scale lengths of the two processes [59]. Clearly a detailed kinetic neutrals model coupled with experimentally constrained recycling distribution will be required to assess and model pedestal fueling and its relationship to the edge transport barrier in setting the pedestal density profile. This also implies that an accurate model of SOL particle transport and recycling will be needed to predict the pedestal density profile of future tokamaks.

## 3.5. PEDESTAL TRANSPORT SCALING

The pedestal density and temperature profiles may also be analyzed to determine the underlying transport controlling the pedestal gradients. In ASDEX-Upgrade the Thomson scattering diagnostic collected data for electron density and temperature in an H-mode pedestal during the quiescent period between ELMs [60-62]. An example of data throughout the ELM cycle from the Thomson diagnostic is shown figure 8. The pedestal electron temperature plotted versus the electron density on a log scale reveals a linear relationship, $\eta_e = d(\ell nT_e)/d(\ell nn_e) = 2$, or the electron density scale length is twice the temperature scale length. This relationship holds throughout the transport suppression region of the pedestal, and throughout the ELM cycle as the profiles evolve. This constant ratio of the temperature and density scale lengths is indicative of drift wave turbulence dominating electron thermal transport. The $\eta_e$ ratio is also seen to generally increase with stronger shaping as theoretical considerations would suggest [62]. A similar scale length ratio has also been observed in DIII-D [63] indicating some universality of this transport mechanism in the pedestal. The scale lengths of the ion temperature and density were also examined in ASDEX-Upgrade [64]. In this case $\eta_i = d(\ell nT_i)/d(\ell nn) = 2$ indicating that ion temperature gradient driven drift modes were not likely responsible for setting the ion temperature profile. Further modeling of these discharges with the fluid code SOLPS indicated that neoclassical ion transport would be sufficient to match the measured ion temperature profile.

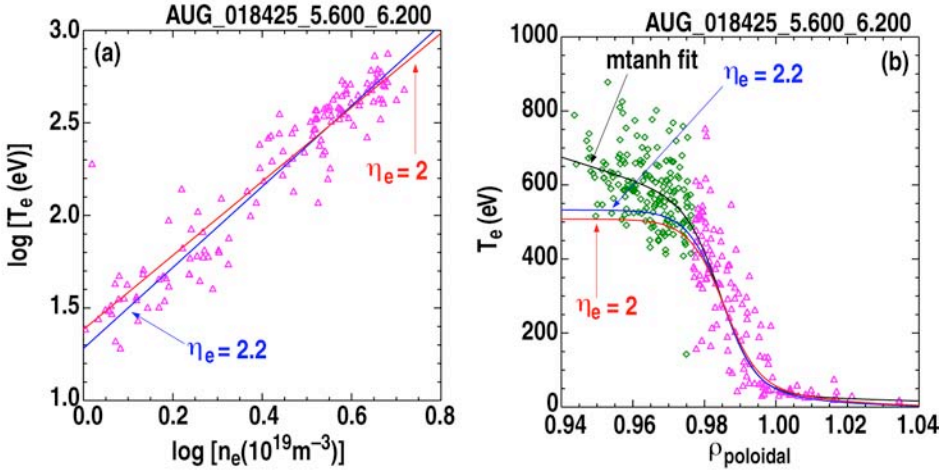


Fig. 8. (a) Linear fit of log(electron temperature) versus log (electron density) in the pedestal region (pink triangles) of a Type I ELMy H-mode. The best fit gives $\eta_e$=2.2, with $\eta_e$=2.0 shown for comparison. (b) Profiles of the edge electron temperature profile; in black a hyperbolic tangential function fit to $T_e$, in blue the assumption of $\eta_e$=2.2, and in red the assumption of $\eta_e$=2.0. (Reprinted with permission from Horton L D 2005 *Nucl Fusion* **45** 856. Copyright 2005, Institute of Physics.)

Pedestal transport can also be characterized by examining trends in the pedestal pressure gradient. In C-Mod a database of pedestal profiles in EDA H-mode was obtained for a range of plasma current, toroidal field and density [65,66]. EDA H-mode in C-Mod is an ELM-free

regime where the typical density rise of H-mode is limited by a quasi-coherent mode (QCM). While there is no consistent variation in the width of the pedestal over the range of parameters examined, clear trends in the pedestal pressure height and gradient are evident. In particular the pedestal pressure and the pressure gradient consistently scale with $I_p^2$. Due to the invariance of the pedestal width across this dataset the pressure gradient exhibited the same $I_p^2$ scaling. This scaling for the pressure gradient is what would be expected for an ideal MHD limit, though these pedestals were computed to be stable to high-$n$ and intermediate-$n$ peeling-ballooning modes. Similar dependencies of the pedestal pressure gradient on $I_p$ have also been observed in ASDEX-Upgrade [61] and JET [67]. These results are consistent with transport being governed by electromagnetic fluid drift turbulence [14,37]. It is possible that both the electrostatic temperature gradient modes as well as electromagnetic turbulence could be active simultaneously in setting the profiles in the edge pedestal.

The profile scaling presented above represents a strong constraint, or crosscheck, of simulation and modeling of pedestal transport. Further work is required to extend this type of analysis to a wider range of parameters, particularly collisionality. The time dependence of the profiles between ELMs must also be examined more closely to determine if the gradients saturate due to this transport with the pedestal width growing until the more global edge MHD limit is approached. Though this analysis highlights the physical mechanisms for transport in the pedestal that models must eventually reproduce, it does not address scaling of the pedestal width needed for projection to future tokamaks.

### 3.6. TOROIDAL FIELD DRIFT DIRECTION

The toroidal field direction has been shown to affect the pedestal structure. This effect may not be unexpected as it is well documented that the H-mode power threshold is considerably reduced when the toroidal field direction is such that the $\nabla B$ drift direction is towards the dominant divertor X-point. In DIII-D with the $\nabla B$ drift towards the X-point the pedestal pressure has been reported higher with less frequent ELMs than for toroidal field in the opposite direction [68]. The higher pressure is primarily a result of higher pedestal density. A similar result has been documented in JET [69]. The dependence of the pedestal height and structure on magnetic field direction is, at this time, mostly anecdotal. Additional experiments and analysis could offer insight into processes that particularly control the pedestal width.

Though scaling of the pedestal with $\nabla B$ drift direction does not significantly aid in pedestal prediction for future burning plasma tokamaks, all are expected to be in the favorable $\nabla B$ configuration to ensure H-mode access, these results do offer insight to the processes controlling the pedestal width. The $\nabla B$ drift direction is known to influence flows in the scrape off layer that could couple flow shear into the pedestal region [70]. On the other hand the toroidal field direction also affects ion orbits that are lost from the pedestal region and potentially alter the region of transport suppression. These are the same issues that arise

when examining the H-mode power threshold dependence on toroidal field direction as will be discussed in section 4.

### 3.7. TOROIDAL FIELD RIPPLE

Toroidal field ripple may also play a role in determining the pedestal profiles. A dimensionless comparison between JET and JT-60U failed to achieve a match of pedestal conditions [71] that was speculated to be due to differences in field ripple. This was also a dimensional comparison with the same discharge size and fields employed in both devices. The attempt to match parameters resulted in a pedestal pressure in JT-60U that was up to 30% lower than in JET, as shown in figure 9, and consequently significantly lower global confinement. The larger toroidal field ripple, ~1.2%, in the edge of JT-60U in the matched shape compared to JET, ~0.1%, became a leading candidate to explain the differences in what should otherwise be identical plasmas. The toroidal field ripple causes a loss of heating beam ions in the edge of JT-60U and results in a toroidal rotation of the plasma counter to the plasma current direction. The JT-60U pedestal could be affected by change to the toroidal rotation profile or perhaps more directly by the beam ion loss altering the radial electric field shear in the edge.

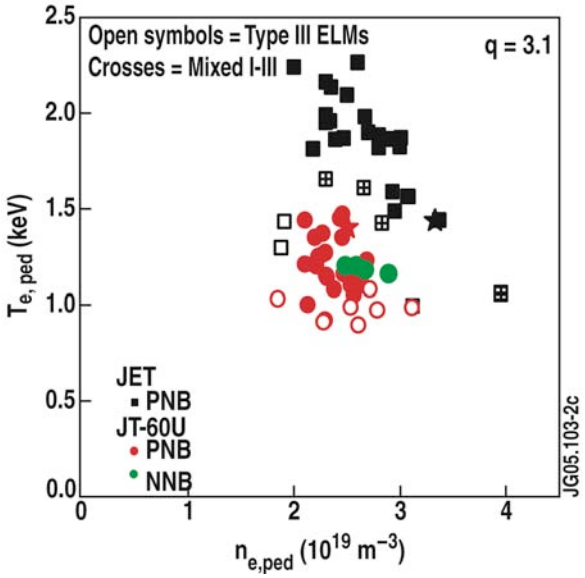


Fig. 9. Comparison of JET and JT-60U pedestal $T_e$ versus $n_e$ (top of the pedestal values), for all similarity discharges at $q_{95}$ = 3.1. The black squares are for JET data, the circles for JT-60U data; red with positive NBI injection and green (large circles) with negative NBI. The stars mark the pedestal values corresponding to the best dimensionless matching points. (Reprinted with permission from Saibene G 2007 *Nucl Fusion* **47** 969. Copyright 2007, Institute of Physics.)

To reduce the toroidal field ripple in JT-60U ferritic steel tiles were installed in the vacuum vessel [72]. These tiles reduced the separatrix averaged field ripple by almost half, from 1.7% to 1.0%, in the large bore configuration and from 0.35% to 0.17% in the smaller

bore configuration. In the larger, higher ripple configuration, the reduced ripple significantly increased the pedestal pressure, ~20%, and global confinement, ~10%. The increase in pedestal pressure was largely a result of an increase in the pedestal width, particularly evident in the ion temperature as the profile of electron temperature was not fully resolved. The improvement in confinement was also accompanied by a reduction in the counter toroidal rotation with respect to the plasma current. For the small bore configuration where the field ripple was well below 1% there was little change to the confinement or rotation with addition of ferritic inserts. The improvements in confinement and pedestal pressure were correlated with both less counter rotation and reduced ion orbit loss.

Complementary experiments at JET have examined the effect of increasing the toroidal field ripple on pedestal and ELM characteristics [73]. A scan of average ripple was performed in JET from its nominal value of 0.08% up to 1% by powering alternating toroidal field coils to differing current levels. Preliminary results indicate that without gas puffing even a modest increase in ripple to 0.3% caused a reduction of pedestal pressure and global confinement of ~15%. The decrease in pedestal pressure was mostly a result of a drop in pedestal density with more rapid ELMs. The pedestal electron and ion temperatures increased, but not enough to overcome the density decrease. The decrease in pedestal pressure and confinement became less with additional gas puffing to raise the density. The JET ripple experiments also found a correlation of increased ripple and reduced pedestal parameters with a shift of toroidal rotation in the direction counter to the plasma current and injected neutral beam momentum. Further work will be required from both JT-60U and JET to determine the respective roles of ion orbit loss and toroidal rotation profile in setting the pedestal structure.

The recent pedestal scaling experiments are quite illuminating, particularly when coupled with the MHD constraints of the peeling-ballooning model. Experiments now showing consistent trends with shape, power, $\beta$, rotation, toroidal ripple and gradients associated with different transport mechanisms will provide a potent test for newly developed models of the pedestal. While most models of the pedestal width are expected to exhibit a significant ion-gyroradius scaling, such scaling has not yet been unambiguously observed in experiment. On the other hand plasma configurations that lead to improved edge stability, such as strong shaping and higher global beta also result in a wider pedestal. This is suggestive of interplay between stability and transport where increased stability results in a higher pressure and greater ion-gyroradius and in turn increases the pedestal width and height. Ion orbit loss may still be playing a role in setting the pedestal width and might be responsible for the observations of pedestal scaling with toroidal ripple and $\nabla B$ drift direction. The observation of critical gradients is an important test for identifying the important transport mechanisms operating in the pedestal. Finally the neutral density is certainly playing a role in setting the pedestal density profile, but its effects on the transport barrier setting the pedestal temperature profiles is mostly unknown.

# 4. H-MODE ACCESS CONDITIONS

The conditions and parameters required to achieve access to H-mode have important implications for both design of future tokamaks and physics understanding of the pedestal structure. Future tokamaks, such as ITER, will require the high confinement of H-mode to achieve burning plasma conditions. Because of the high cost of heating systems it will be important to have an accurate prediction of the required auxiliary heating power required to achieve the H-mode transition. In addition an understanding of the conditions required for H-mode access adds insight to the processes that control the pedestal structure, particularly the width of the H-mode transport suppression region.

The ITPA Confinement Database and Modeling topical group has had an ongoing database effort to parameterize the H-mode power threshold [74]. Analysis of data from six of the larger tokamaks produced a power threshold scaling similar to previous studies with increasing power threshold at higher density and field. This scaling indicates that for ITER operating at its full field and a low density of $0.5\times10^{20}\,\mathrm{m}^{-3}$, 55 MW of additional heating should be sufficient to achieve H-mode. However at a higher density of $1.0\times10^{20}\,\mathrm{m}^{-3}$ the expected required auxiliary power rises to 95 MW. Significant uncertainties remain in that analysis from single devices produces a stronger density dependence than the combined scaling. This may lead to a higher power threshold than the scaling indicates at the higher densities of ITER. Also a number of machines find a minimum density for the power threshold scaling before the power threshold begins increasing. This lower density limit may increase with toroidal field and would indicate a higher minimum density and power threshold in ITER. Also the minimum power above the threshold required to achieve good confinement has been examined, but no firm conclusion can yet be drawn for this aspect of H-mode operation.

The correlation of H-mode power threshold and plasma rotation has come under increased study recently. It has long been observed that the H-mode power threshold is significantly lower when the $B\times\nabla B$ drift direction is towards the dominant X-point [75-76]. The power threshold can be even lower when the magnetic configuration is very near to a balanced double-null, as shown by results from ASDEX-Upgrade and MAST [77]. A correlation between the radial electric field of H-mode and SOL plasma flows has been examined theoretically by Rozhansky [78]. Examining both these issues together plasma flows were measured in the C-Mod SOL for USN and LSN configurations while the toroidal field and plasma current were kept constant [70]. In the USN configuration the $\nabla B$ drift direction was downward away from the X-point and resulted in an H-mode power threshold about a factor of two higher than the LSN configuration. When the plasma current and toroidal field were reversed in direction the LSN configuration exhibited the higher power threshold indicating the significance of the $\nabla B$ drift direction. In all configurations plasma in the SOL was carried by parallel flow from the outboard midplane around the periphery of the

plasma to the inboard divertor. The toroidal component of these flows was always in the direction of the plasma current for the favorable $\nabla B$ drift direction and counter to the current in the unfavorable $\nabla B$ drift direction. The core rotation in ohmic plasmas is counter to the plasma current in all configurations, with the greatest counter rotation for the unfavorable $\nabla B$ drift direction, consistent with the edge toroidal rotation providing a boundary condition for the bulk plasma rotation. In H-mode as the stored energy increases the core rotation shifts toward the plasma current direction. The C-mod data suggests that in the favorable $\nabla B$ drift direction the SOL flows couple to plasma inside the separatrix and shift the toroidal rotation towards that more favorable for H-mode access. The edge electron temperature at the H-mode transition was also found to be higher in the unfavorable configuration. This lends support to the concept that the transition is triggered by shear in the $E \times B$ flows rather than the gradients in the temperature and density profiles directly.

In DIII-D the H-mode power threshold was examined by varying the central torque with co and counter neutral beam injection [79]. The power threshold was found to be significantly lower with more counter injection torque. The reduction in power was most significant with the toroidal field in the unfavorable $\nabla B$ drift direction. Also the edge fluctuation levels in L-mode were found to be lower with the counter injection compared to co injection at the same power level. This is in contrast to the C-Mod results where lower power thresholds were associated with core rotation more in the co direction with the plasma current.

The leading paradigm for the H-mode transition is still that when the shear in the edge radial electric field, or $E \times B$ flow shear, exceeds a threshold value turbulent transport is suppressed leading to higher edge pressure gradients and in turn greater flow shear. While the edge pressure may be responsible for part of this shear, toroidal momentum transport may also play an important role in establishing the sheared flow required for the H-mode transition. Still unresolved is the role ion orbit loss or neoclassical transport may play in establishing the $E \times B$ flow shear observed. Experiments are needed to separate the effects of ion orbit loss from direct momentum transport in establishing the required shear flow for the H-mode transition.

# 5. SUMMARY AND CONCLUSIONS

There has been significant recent progress in the experimental characterization and modeling of pedestal structure. A number of models under development will be capable of taking into account a number of physical effects of the pedestal region that are important, including shaping, full gyrokinetic turbulence, self-consistent neoclassical transport, collisionality and neutral particle sources. Detailed experimental testing of these codes will be required to provide confidence in using them for prediction of future burning plasma tokamak performance.

The pedestal models should be tested through two exercises: 1) prediction of experimentally measured profiles, including fluxes and fluctuations, and 2) reproduction of experimentally observed scaling trends. Obtaining adequate experimental measurements for these tests provides significant challenges that must be overcome. One of the more challenging of these measurements is that of the particle source profile. Knowledge of the particle source, derived from the neutral density profile, is one of the fundamental characteristics of a transport system that must be determined to test any model of that system. There are reasonable prospects for measuring the 2D neutral density profile, but it requires additional resources through extending coverage of existing diagnostics and extensive interpretive modeling. Measurement of the neutral density profile will also provide other benefits, such as determination of charge-exchange losses. Other diagnostic improvements that are required are more straightforward but will require significant additional resources. These improvements include measuring the profiles of all species in each tokamak with sufficient spatial resolution to resolve the pedestal and sufficient time resolution to follow evolution of the profiles between ELMs. Finally a few other diagnostics that have been primarily developed for the core, particularly fluctuation and current profile diagnostics, will also have to be adapted for the pedestal and its spatial and temporal resolution issues.

While the pedestal scaling results have been very illuminating several areas still require further, careful experimental measurements. Of very high priority is the scaling of the pedestal with the ion gyroradius. This is one parameter of future burning plasma tokamaks that cannot be matched in current experiments. Because of this, predictions of the pedestal in future tokamaks rely on extrapolation of experimental trends and validation of the ion gyroradius physics in the predictive model. Also the ion gyroradius is fundamental to theories that rely on $E \times B$ flow shear stabilization of turbulent transport to establish the width of the pedestal. Models under development are expected to exhibit this scaling. If the lack of ion-gyroradius dependence observed in a few initial experiments is confirmed by further experiment and modeling this result will have significant implications for scaling current tokamak performance to future larger tokamaks such as ITER. Because of its implications further experiments to study gyroradius scaling should be given a higher

priority. These studies should also be coordinated across devices of varying size to increase the range of gyroradius values examined.

There are also other mechanisms that may play a role in the pedestal structure that still need to be examined. Unlike current devices particle recycling will contribute very little to the particle source of the pedestal in ITER because of the high density and longer path lengths. Because of this central fueling with pellets will provide most of the ion flux through the pedestal. Efforts should be made to test the effects of such ion flux on the pedestal structure, particularly the density profile. The pedestal width was found to increase with power and/or global beta, but their relative importance has not yet been determined. While these two parameters are typically very well correlated they might be separated by comparing discharges in two different confinement regimes while other parameters are held constant. Finally pedestal collisionality, which has implications for turbulent transport, should also be examined. The challenge of isolating this parameter experimentally is that the pedestal bootstrap current, and the resulting magnetic shear, is strongly correlated with the collisionality over typical parameters of current devices. A scan of low collisionality, though, where the bootstrap current is not so dependent may be beneficial.

The H-mode power threshold requirement is also a very important issue in the context of pedestal research. The power requirement to achieve H-mode is an important design issue for burning plasma tokamaks and reducing uncertainty can result in significant cost savings. A better understanding of the threshold conditions is also likely to illuminate mechanisms controlling the pedestal width. Recent results indicate a coupling of toroidal momentum to shear in the edge electric field. Ion orbit losses may also be playing a role. These results coupled with further L-H transition database work could result in reduced uncertainty in predicting the requirements for achieving H-mode.

# REFERENCES


[1] Hubbard A E 2000 *Plasma Phys Control Fusion* **42** A15

[2] Hatae T, Sugihara M and Hubbard A E 2001 *Nucl Fusion* **41** 285

[3] Wilson H R, Snyder P B, Huysmans G T A, Miller R L 2002 *Phys Plasmas* **9** 1277

[4] Snyder P B, Wilson H R, Ferron J R, Lao L L, Leonard A W, Mossessian D, Murakami M, Osborne T H, Turnbull A D and Xu X Q 2004 *Nucl Fusion* **44** 320

[5] Snyder P B, Wilson H R, Osborne T H and Leonard A W 2004 *Plasma Phys Control Fusion* **46** A131

[6] Hatae T, 2001 *Nucl. Fusion* **41** 285

[7] Osborne T H *et al* 2002 *Proc 19th IAEA Fusion Energy Conference (Lyon)* IAEA-CN-94/CT-3

[8] Sugihara M, Mukhovatov V, Polevoi A and Shimada M 2003 *Plasma Phys Control Fusion* **45** L55

[9] Cordey J G for the ITPA H-Mode Database Working Group and the ITPA Pedestal Database Working Group 2003 *Nucl Fusion* **43** 670

[10] Onjun T, Bateman G, Kritz A H and Hammett G 2002 *Phys Plasmas* **9** 5018

[11] Staebler G M, Kinsey J E and Waltz R E 2005 *Phys Plasmas* **12** 102508

[12] Staebler G M, Kinsey J E and Waltz R E 2006 *Proc 21st IAEA Fusion Energy Conference (Chengdu)* IAEA-CN-149/TH/1-2

[13] Scott B 2000 *Phys Plasmas* **7** 1845

[14] Scott B 2005 *Phys Plasmas* **12** 102307

[15] Xu X Q *et al* 2007 *Nucl Fusion* **47** 809

[16] Chang C S, Seunghoe Ku and Weitzner H 2004 *Phys Plasmas* **11** 2649

[17] Chang C S *et al* 2006 *Proc 21st IAEA Fusion Energy Conference (Chengdu)* IAEA-CN-149/TH/P6-14

[18] Coster D P *et al* 2002 *Proc 19th IAEA Fusion Energy Conference (Lyon)* IAEA-CN-94/THP2/13

[19] Rognlien T, Milovich J, Rensink M and Porter G 1992 *J Nucl Mater* **196-198** 347

[20] Simonini R, Corrigan G, Radford G, Spence J and Taroni A 1994 *Contrib. Plasma Phys.* **34** 368

[21] Stacey W M and Groebner R J 2007 *Phys Plasmas* **14** 012501

[22] Stacey W M submitted to Phys Plasmas

[23] Degeling A W, Weisen H, Zabolotsky A, Duval B P, Pitts R A, Wischmeier M, Lavanchy P, Marmillod Ph and Pochn G 2004 Rev Sci Instrum **75** 4139

[24] Whyte D G, Lipschultz B L, Stangeby P C, Boedo J, Rudakov D L, Watkins J G and West W P 2005 *Plasma Phys Control Fusion* **47** 1579

[25] Lipschultz B, Whyte D and LaBombard B 2005 *Plasma Phys Control Fusion* **47** 1559

[26] Leonard A W, Boedo J A, Groth M, Lipschultz B L, Porter G D, Rudakov D L and Whyte D G 2007 *J Nucl Mater* **363-365** 1066

[27] Stangeby P C 2002 "The Plasma Boundary of Magnetic Fusion Devices", Institute of Physics, Bristol

[28] Groth M *et al* 2005 *J Nucl Mater* **337-339** 425

[29] Porter G D, Casper T A, Moller J M 2001 *Phys Plasmas* **8** 5140

[30] Moyer R A, Tynan G R, Holland C and Burin M J 2001 *Phys Rev Lett* **87** 135001

[31] Kurzan B, *et al* 2007 *Plasma Phys Control Fusion* **49** 825

[32] Shirmer J, *et al* 2007 *Plasma Phys Control Fusion* **49** 1019

[33] Sugihara M, Igitkhanov Yu, Janeschitz G, Hubbard A E, Kamada Y, Lingertat J, Osborne T H and Suttrop W 2000 *Nucl Fusion* **40** 1743

[34] Sauter O, Angioni C and Lin-Liu Y R 1999 *Plasmas* **6** 2834

[35] Wade M R, Murakami M and Politzer P A 2004 *Phys Rev Lett* **92** 235005

[36] Thomas D M, Leonard A W, Groebner R J, Osborne T H, Casper T A, Snyder P B and Lao L L 2005 *Phys Plasmas* **12** 056123

[37] Rogers B N and Drake J F 1999 *Phys Plasmas* **6** 2797

[38] Hinton F L and Staebler G M 1993 *Phys Fluids B* **5** 1281

[39] Shaing K C 1992 *Phys Fluids B* **4** 290

[40] Chang C S, Seunghoe Ku and Weitzner H 2004 *Phys Plasmas* **11** 2649

[41] Osborne T H, Groebner R J, Lao L L, Leonard A W, Maingi R, Miller R L, Porter G D, Thomas D M and Waltz R E 1998 *Plasma Phys Control Fusion* **40** 845

[42] Groebner R J, Mahdavi M A, Leonard A W, Osborne T H, Porter G D, Colchin R J and Owen L W 2002 *Phys Plasmas* **9** 2134

[43] Fenstermacher M E *et al* 2005 *Nucl Fusion* **45** 1493

[44] Mossessian D A, Groebner R J, Moyer R A, Osborne T H, Hughes J W, Greenwald M, Hubbard A and Rhodes T L 2003 *Phys Plasmas* **10** 689

[45] Kallenbach A *et al* 2002 *Nucl Fusion* **45** 1493

[46] Maggi C F *et al* 2007 *Nucl Fusion* **47** 535

[47] Snyder P B *et al* 2007 *Nucl Fusion* **47** 961

[48] Kamada Y, Takenaga H, Isayama A, Hatae T, Urano H, Kubo H, Takizuka T and Miura Y 2002 *Plasma Phys Control Fusion* **44** A279

[49] Leonard A W, Casper T A, Groebner R J, Osborne T H, Snyder P B and Thomas D M 2007 *Nucl Fusion* **47** 552

[50] Saibene G *et al* 2002 *Plasma Phys Control Fusion* **44** 1769

[51] Kamada Y and the JT-60 Team 1999 *Plasma Phys Control Fusion* **41** B77

[52] Stober J, Gruber O, Kallenbach A, Mertens V, Ryter F, Stäbler A, Suttrop W, Treutterer W and the ASDEX Upgrade Team 2000 *Plasma Phys Control Fusion* **42** A211

[53] Mahdavi M A, Maingi R, Groebner R J, Leonard A W, Osborne T H and Porter G 2003 *Phys Plasmas* **10** 3984

[54] Nunes I *et al* 2004 *Proc. 31st EPS Conference on Plasma Physics (London)* Vol 28B (ECA) P4.137

[55] Kallenbach A *et al* 2004 *Plasma Phys Control Fusion* **46** 431

[56] Kirk A, Counsell G F, Arends E, Meyer H, Taylor D, Valovic M, Walsh M, Wilson H and the MAST Team 2004 *Plasma Phys Control Fusion* **46** A187

[57] Hughes J W, LaBombard B, Mossessian D A, Hubbard A E, Terry J, Biewer T and the Alcator C-Mod Team 2006 *Phys Plasmas* **13** 056103

[58] Hughes J W, LaBombard B, Terry J, Hubbard A and Lipschultz B 2007 *Nucl Fusion* **47** 1057

[59] Owen L W, *et al* 2005 *J Nucl Mater* **337-339** 410

[60] Horton L D *et al* 2005 *Nucl Fusion* **45** 856

[61] Neuhauser J *et al* 2002 *Plasma Phys Control Fusion* **44** 855

[62] Kurzan B *et al* 2007 *Proc 33rd EPS Conference on Plasma Physics (Warsaw)*

[63] Groebner R J, Leonard A W, Luce T C, Fenstermacher M E, Jackson G L, Osborne T H, Thomas D M and Wade M R 2006 *Plasma Phys Control Fusion* **48** A109

[64] Wolfrum E *et al* 2007 *Proc 33rd EPS Conference on Plasma Physics (Warsaw)* Vol 28B

[65] Hughes J W *et al* 2007 Fusion Sci Technol 51 317

[66] Hubbard A E *et al* 2007 *Phys Plasmas* **14** 056109

[67] Loarte A *et al* 2004 *Phys Plasmas* **11** 2668

[68] Petrie T W *et al* 2003 J Nucl Mater 313-316 834

[69] Loarte A *et al* 2005 *Proc 32nd EPS Conference on Plasma Physics (Taragona)* Vol 29C, P-2.007

[70] LaBombard B *et al* 2005 *Phys Plasmas* **12** 056111

[71] Saibene G *et al* 2007 *Nucl Fusion* **47** 969

[72] Urano H, Oyama N, Kamiya K, Koide Y, Takenaga H, Takizuka T, Yoshida M, Kamada Y and the JT-60 Team 2007 *Nucl Fusion* **47** 706

[73] Sartori R *et al* 2007, this conference

[74] Martin Y R *et al* 2007, this conference

[75] Wagner F, *et al* 1985 *Nucl Fusion* **25** 1490

[76] Carlstrom T N *et al* 1994 *Plasma Phys Control Fusion* **36** A147

[77] Meyer H *et al* 2006 *Nucl Fusion* **46** 64

[78] Rozhansky V *et al* 2007 *J Nucl Mater* **363-365** 664

[79] Gohil P, McKee G R, Wang G, Ferron J R, Kinsey J E, Petty C C and Schlossberg D J 2007, this conference

## ACKNOWLEDGMENT

This work was supported in part by the U.S. Department of Energy under Cooperative Agreement DE-FC02-04ER54698.